Acta Oceanol. Sin., 2024, Vol. 43, No. 9, P. 81–92
https://doi.org/10.1007/s13131-024-2364-1
http://www.aosocean.com
E-mail: ocean2@hyxb.org.cn

Changes in area fraction of sediment-laden sea ice in the Arctic Ocean during 2000 to 2021

Yuanyang Xie[1, 2, 3], Tingting Liu[1, 2, 3], Na Li[3], Ruibo Lei[1, 3*]

[1] Chinese Antarctic Center of Surveying and Mapping, Wuhan University, Wuhan 430079, China

[2] Key Laboratory of Polar Environment Monitoring and Public Governance, Wuhan University, Wuhan 430079, China

[3] MNR Key Laboratory for Polar Science, Polar Research Institute of China, Shanghai 200136, China

Received 28 February 2024; accepted 25 April 2024

Abstract

Sediment-laden sea ice plays an important role in Arctic sediment transport and biogeochemical cycles, as well as the shortwave radiation budget and melt onset of ice surface. However, at present, there is a lack of efficient observation approach from both space and *in situ* for the coverage of Arctic sediment-laden sea ice. Thus, both spatial distribution and long-term changes in area fraction of such ice floes are still unclear. This study proposes a new classification method to extract Arctic sediment-laden sea ice on the basic of the difference in spectral characteristics between sediment-laden sea ice and clean sea ice in the visible band using the MOD09A1 data with the resolution of 500 m, and obtains its area fraction over the pan Arctic Ocean during 2000–2021. Compared with Landsat-8 true color verification images with a resolution of 30 m, the overall accuracy of our classification method is 92.3%, and the Kappa coefficient is 0.84. The impact of clouds on the results of recognition and spatiotemporal changes of sediment-laden sea ice is relatively small from June to July, compared to that in May or August. Spatially, sediment-laden sea ice mostly appears over the marginal seas of the Arctic Ocean, especially the continental shelf of Chukchi Sea and the Siberian seas. Associated with the retreat of Arctic sea ice extent, the total area of sediment-laden sea ice in June–July also shows a significant decreasing trend of 8.99×10^4 km^2 per year. The occurrence of sediment-laden sea ice over the Arctic Ocean in June–July leads to the reduce of surface albedo over the ice-covered ocean by 14.1%. This study will help thoroughly understanding of the role of sediment-laden sea ice in the evolution of Arctic climate system and marine ecological environment, as well as the heat budget and mass balance of sea ice itself.

Key words: sea ice, sediments, optical remote sensing, Arctic Ocean

Citation: Xie Yuanyang, Liu Tingting, Li Na, Lei Ruibo. 2024. Changes in area fraction of sediment-laden sea ice in the Arctic Ocean during 2000 to 2021. Acta Oceanologica Sinica, 43(9): 81–92, doi: 10.1007/s13131-024-2364-1

1 Introduction

Sediment-laden sea ice, also known as “dirty ice”, generally refers to sea ice rich in sediment components, mainly of silt and algae (Simpkins, 2020). Seafloor or runoff-carried sediments are the primary source of particles entrained in sea ice during its initial growth stage, mainly through underwater interaction between frazil ice and resuspended sediments, which is referred to as suspension freezing (Ito et al., 2019). Algae also enter the sea ice during the process of suspension freezing. Ice algal communities live at the ice/water interface, flooded surface, or in interior layers of ice column, giving heavily colonized sea ice its distinctive brown color (Arrigo, 2014). Mammals, especially seals and walruses, may also bring some suspended matters from seawater to the ice surface, which would subsequently remain there until the ice melts over (Laidre et al., 2008). In addition, the sediments can also be enriched on the partially low-lying surface of the sea ice caused by the horizontal migration of surface melt water during the summer (Nomura et al., 2010). The Arctic continental shelf is a major site for sea ice formation (Cornish et al., 2022), especially the Beaufort-Chukchi seas and the Siberian seas, where the water is often rich in suspended matter because of the river runoff and ocean entrainment due to the shallow water (Eicken et al., 2005), and the activities of mammals are more frequent, especially during the ice melt season. Thus, sediment-laden sea ice was often observed in these regions (Darby et al., 2011; Lei et al., 2017). For instance, based on ship-based observations, the proportion of sediment-laden sea ice in the Chukchi Sea can reach 50%–60% in summer (Lei et al., 2017; Tucker et al., 1999). In addition, large areas of sediment-laden sea ice, which often form locally in shallow waters, had also been observed in Canada Hudson Bay (Barber et al., 2021).

Sea ice advection in the Arctic Ocean plays an important role in the material redistributions, greatly impacting the basin-scale biogeochemical cycles. From an ecological perspective, sediment-laden sea ice serves as a carrier for the biogenic elements or pollutants, transporting them between locations from the Arc-

Foundation item: The National Key Research and Development Program of China under contract No. 2021YFC2803304; the National Natural Science Foundation of China under contract No. 42325604; the Program of Shanghai Academic/Technology Research Leader under contract No. 22XD1403600; the Fundamental Research Funds for the Central Universities under contract No. 2042024kf0037; the Fund of Key Laboratory for Polar Science, Ministry of Natural Resources, Polar Research Institute of China, under contract No. KP202004.

*Corresponding author, E-mail: leiruibo@pric.org.cn

tic continental shelf where the ice initially forms to the deep basins or even out of the Arctic Ocean where the ice finally melts (Pfirman et al., 1995; Holmes et al., 2002; Krumpen et al., 2019). Specifically, sediments incorporated into sea ice are an important source of iron and nutrients released during ice melt and support phytoplankton growth, thereby stimulating the marine primary productivity (Kanna et al., 2014). As Arctic sea ice thins, the retention time of sea ice in advection over the Arctic basin may be shortened (Krumpen et al., 2019; Sumata et al., 2023), and the response of sea ice motion to wind forcing can be strengthened (Zhang et al., 2022). These factors have the potential to change the transport path and spatial distribution of the sediment-laden ice, as well as the fate of sediments carried by the ice, thereby affecting the ecosystem over the pan Arctic Ocean. Due to its apparent spectral characteristics of gray-brown, sediment-laden sea ice has relatively low surface reflectivity, so compared to normal clean ice or snow-covered ice, it can absorb more solar shortwave radiation, which is the main component of heat balance on sea ice surface in summer (Ledley and Pfirman, 1997).

In field observations, ice core extraction is a common method to determine the concentration of sediment within the ice (Stierle and Eicken, 2002; Wegner et al., 2017). In addition, sediment-laden sea ice can also be directly observed through the spectral measurements over sea ice surfaces (Light et al., 2022) and the ship-based visual observation or camera monitoring (Lei et al., 2017). Field observations can provide accurate surface reflectance, which is crucial to construct the optical model of sea ice (Light et al., 1998). However, data obtained from field observations, whether from ship-based observations or ice sampling on the ice stations, can only provide snapshot observations and lack spatial coverage, which restricted the acquisition of basin-scale spatial distribution and long-term changes in this special and important sea ice. Moreover, ship-based observations usually overlook the shallow-water nearshore regions, which are often rich in the sediment-laden ice. The influence of sediment components on the spectral characteristics of sea ice, especially for the reflectivity, is mainly in the visible bands of the light spectrum. Therefore, the optical remote sensing data should have great potential in identifying sediment-laden sea ice. The optical remote sensing can provide large-scale observations of sea ice geophysical parameters over the Arctic Ocean, which has been used to discriminate sea ice surface types (Eicken et al., 2000; Huck et al., 2007), melt pond (Markus et al., 2003; Webster et al., 2015), and extract sea ice form sediment-laden seawater (Zhang et al., 2015). However, due to the challenges of accurate extraction of sediment-laden sea ice caused by the cloud contamination, snow cover, and lack of validation data, time series products for facilitating trend analysis of sediment-laden sea ice over the entire Arctic Ocean are still lacking. Therefore, in order to gain a full-picture understanding of the spatial distribution and long-term changes of sediment-laden ice in the Arctic Ocean, and to characterize the spatial transport of sediments and the heat balance of the ice surface, it is necessary to develop an algorithm to obtain time series product of area fraction of sediment-laden sea ice at the basin scale using the satellite optical observations.

Various optical satellite images are available in the Arctic Ocean. The Advanced Visible High Resolution Radiometer (AVHRR) only has a single visible band at 580–680 nm (Brest and Rossow, 1992), which limits the construction of the algorithm to recognize sediment-laden ice from the ordinary ice. Furthermore, its spatial resolution of 1.1 km is relatively low to obtain the spectral characteristics over the discrete floes in the melt season. For the Landsat-8 and the Sentinel-2, the revisit period in the Arctic region is longer than 3 d (Irons et al., 2012) and 5 d (Drusch et al., 2012), respectively. In addition, both Landsat-8 and Sentinel-2 images cannot cover the entire Arctic region. These disadvantages limit the construction of the pan-Arctic products, and given the cloud contamination, it may result in large spatiotemporal gaps in the time series. In contrast, Moderate-resolution Imaging Spectroradiometer (MODIS) has more spectral bands and higher spatiotemporal resolution compared to the AVHRR, and its images can cover a larger region over the entire Arctic region compared to the Landsat-8 and the Sentinel-2 (Rösel et al., 2012). Furthermore, the MODIS images have been available since 2000, which can provide relative long time series observations for the diagnosis of long-term changes in Arctic surface features.

In this paper, we design a new classification method and apply it to the MODIS data to extract sediment-laden sea ice in the Arctic Ocean. Based on 22 years of data during 2000 to 2021, we determined the main distribution areas of sediment-laden sea ice, and discussed the potential relationship between temporal variations in Arctic sediment-laden sea ice area fraction and changes in summer Arctic sea ice extent. And then we also elucidated the impacts of sediments on surface albedo and shortwave radiation budget of sea ice. Landsat-8 true color images with a resolution of 30 m and optical images obtained from ship-based measurements were used to verify the classification results. The remainder of this paper is organized as follows: Section 2 describes the MODIS data and other datasets employed for validation and analysis; Section 3 describes the classification method for sediment-laden sea ice; Section 4 quantifies the accuracy of classification method and analyzes the spatial distribution and temporal variations of sediment-laden sea ice; Section 5 provides a summary; Section 6 provides the outlook of this study.

2 Data

2.1 *MODIS data*

MODIS was launched with the Earth Observation System's Terra AM satellite in 1999, and with another Earth Observation System's Aqua PM satellite in 2002. Terra MODIS and Aqua MODIS are viewing the entire Earth's surface every one to two days, acquiring data in 36 spectral bands from 0.4 μm to 14.4 μm. The spatial resolution of MODIS is 250 m at Bands 1–2, 500 m at Bands 3–7, and 1 000 m at Bands 8–36, respectively. The scan width of MODIS is 2 330 km. According to the processing level, MODIS data products are divided into level 0 original products to level 5 products developed based on various application models.

In this study, surface reflectance product MOD09A1 (Vermote, 2021) is used, which provides MODIS surface reflectance at Bands 1–7 with a 500 m resolution, approximately the scale of moderate to large ice floes in the marginal ice zone of Arctic Ocean during summer (Lei et al., 2017). The product at each pixel contains the best possible observation over an 8-d period, selected on the basis of high observation coverage, low view angle, absence of clouds or cloud shadow, and aerosol loading. This can greatly reduce the impact of clouds and cloud shadows on surface reflection observations. The MOD09A1 data set used here is provided by the U.S. National Aeronautics and Space Administration (NASA) and archived at the Atmosphere Archive & Distribution System Distributed Active Archive Center at https://ladsweb.modaps.eosdis.nasa.gov/ (last access: February 25, 2024).

First, the images on the same date are mosaiced, projected, resampled in sequence from the initial sinusoidal projection to polar stereographic projection under the WGS84 coordinate sys-

tem using the MODIS Reprojection Tool (MRT) provided by the NASA. Then, the image is cropped to ensure the coverage of the entire Arctic Ocean, which served as the study area (Fig. 1). The 500-m state flags data information, contained in the attribute lookup table of the data product, was used to identify clouds and land at each pixel. Prior to early May, the surface of Arctic sea ice is generally covered with relatively thick snow (Bliss and Anderson, 2018), which would affect the identification of dirty ice, with sediment enrichment on the ice/snow interface. After mid-September, there would be large areas of MODIS data missing in the visible band over the central Arctic Ocean. Therefore, the period from early May to early September is defined as the study period in this study, and the MODIS data obtain from this period were used for the extraction of sediment-laden sea ice over the Arctic Ocean and the subsequent analysis of its spatial distribution and long-term change during 2000 to 2021. This study period is also crucial for the shortwave radiation budget and melt of Arctic sea ice surface (Perovich et al., 2002; Lei et al., 2016).

2.2 *Landsat-8 OLI*

The spatial resolution of Landsat-8 Operational Land Imager (OLI) visible bands is 30 m, which is smaller than or comparable with most patch sizes of sediment-laden ice, generally with a diameter of several dozen meters according to the ship-based visual observation. It implies that the Landsat data can be used to validate the area fraction of sediment-laden ice retrieval from the MODIS. The OLI data of Landsat-8 is provided by the NASA and available at the website of United States Geological Survey at https://earthexplorer.usgs.gov/ (last access: February 25, 2024) .

Here the Landsat-8 data collected from the end of May to early August during 2017 to 2021 were used as ground truth data. In total 1 411 scenes of Landsat-8 data are used in this study. These images cover most of the coastal regions in the Arctic Ocean (Fig. 2), where sediment-laden sea ice is often observed.

2.3 *Ship-based photos from R/V Xuelong*

During the 9th Chinese National Arctic Research Expedition carried out in summer 2018 (CHINARE-2018), two cameras were fixed on the port and starboard sides of R/V *Xuelong* to automatically and continuously monitor the ice conditions every 5 min. In total 27 photographs taken on board in early August were used to verify the sediment-laden sea ice classification results in this study, which were obtained during the R/V *Xuelong*

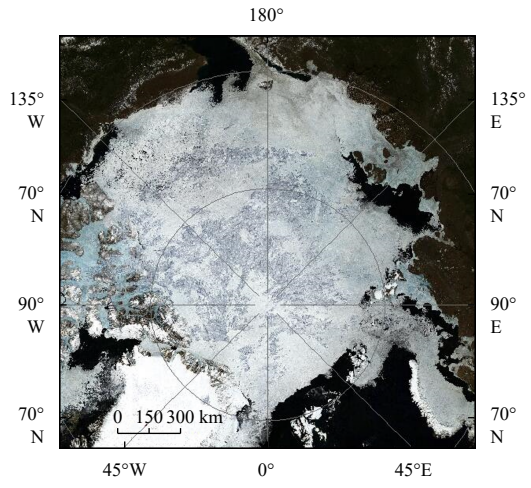

Fig. 1. A resized true color MOD09A1 image over the Arctic on June 18, 2018.

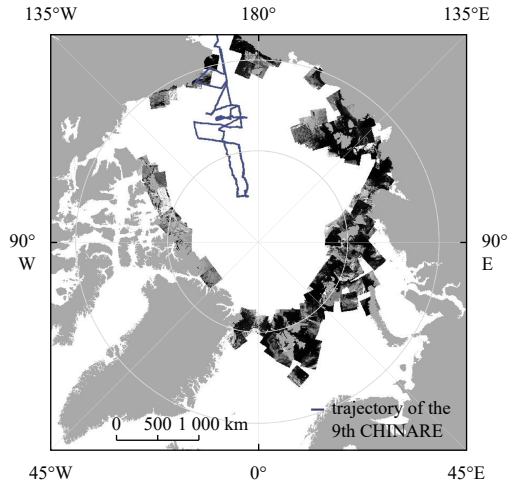

Fig. 2. Coverage of Landsat-8 images used as ground truth data in 2018 and the trajectory of the 9th Chinese National Arctic Research Expedition (CHINARE) during July–September 2018.

sailing through the southern Chukchi Sea, with sea ice rich in sediment.

2.4 *NSIDC ice extent*

To explore the effect of cloud on the classification results, Arctic sea ice extent provided by the National Snow and Ice Data Center (NSIDC) at https://nsidc.org/ (last access: February 25, 2024) was used and compared with the result derived from MOD09A1 data. In addition, we used the minimum Arctic sea ice extent in September to explore its relationship with the changes in the area fraction of sediment-laden sea ice in early summer.

2.5 *IBCAO chart*

To investigate the main source areas of sediment-laden sea ice, the relationship between the distribution of sediment-laden sea ice and seafloor topography were analyzed using the data provided by the International Bathymetric Chart of the Arctic Ocean (IBCAO) (Jakobsson et al., 2020). Its latest version 4.2 with a resolution of 200 m, available at https://www.gebco.net/ (last access: February 25, 2024), is used in this study.

3 Methods

Within the study area (Fig. 1), five components of land, clouds, open water, clean sea ice, and sediment-laden sea ice, are considered. After the classification and extraction of land and clouds, the forward simulated reflectance was applied to further identify open water, clean ice, and sediment-laden ice according to their spectral properties.

3.1 *Forward simulated reflectance*

The spectral reflectance of various surface features, and the corresponding relationship between reflectance and a given surface feature can be simulated using a physical model (Waga et al., 2022). By assuming the vertical stratification and horizontal homogeneity, a structural optical model (Light et al., 1998) and a radiative transfer model for sea ice with vertical layered structure (Grenfell, 1991) were used to simulate spectral reflectance of various ice surface types (Waga et al., 2022). According to Waga et al. (2022), four surface features of open water, clean sea ice, sea ice with low sediment content (50 g/m^3), and sea ice with high sediment content (500 g/m^3) were defined and classified in this

study. The simulated surface reflectance of various surface features for 7 visible bands of MODIS are presented in Fig. 3.

As shown in Fig. 3, the major difference in reflectance of various surface features is in the visible band. Especially at Band 3 of 459–479 nm, the reflectance ranges from 0.1 for open water to 0.9 for clean ice.

3.2 *Extraction of open water*

Generally, open water has a significantly higher absorption rate than other surface features in the visible band (McFeeters, 1996), and the reflectance of open water is usually less than 0.1 in visible band (Ji et al., 2009), which is consistent with our simulation results as shown in Fig. 3. Therefore, open water and sea ice can firstly be distinguished based on the differences of their spectral characteristics in visible band. Here we set a threshold (0.15) of the averaged reflectance of Bands 1, 3, and 4 to extract open water from the MODIS images.

3.3 *Extraction of clean sea ice and sediment-laden sea ice*

The difference in spectral characteristics between clean sea ice and sediment-laden sea ice is mainly caused by the sediment components (Ledley and Pfirman, 1997). When silt, algae and other components in the sediment are enriched on the upper surface of sea ice, the spectral absorptivity of sea ice surface will be enhanced, resulting in a reduction in ice surface reflectivity and a darker area in the images. The influence of these sediment components on the spectral characteristic is mainly in the visible bands, corresponding to Bands 1, 3, and 4 of MODIS. For Bands 2, 5, 6, and 7 of MODIS, the sediment composition has little effect on reflectivity due to the strong absorption characteristics of sea ice itself. When analyzing the spectral characteristics of water with different sediment contents, Band 3 of MODIS is the main absorption band of sediment components, and Band 4 is an insensitive band (Fang and Zhang, 2007). Similar to the mineral sediment, algae in water also have similar effects on spectral characteristics in the visible bands. Thereby, as shown in Fig. 3, the surface reflectance of sediment-laden sea ice, both for low and high enrichment levels, shows a distinct increase from Band 3 (blue, 459–479 nm) to Band 4 (green, 545–565 nm) and a decrease to Band 1 (red, 620–670 nm), significantly different from the clean sea ice. Furthermore, near the Band 2 (infrared, 841–867 nm), sea ice with low sediment content or clean surface shows the similar surface reflectance characteristics.

Based on the relatively high absorption ratio of sediment components in the visible bands compared to clean sea ice, the reflectivity of MODIS Bands 1, 3, and 4, (R_1, R_3, and R_4) were selected and used to define the classification indices R_{13}, R_{14}, and R_{34} as follows:

$$R_{13} = (R_3 - R_1)/(R_3 + R_1), \tag{1}$$

$$R_{14} = (R_4 - R_1)/(R_4 + R_1), \tag{2}$$

$$R_{34} = (R_4 - R_3)/(R_4 + R_3). \tag{3}$$

Three mixed pixel cases, including (1) general case, (2) clean ice and sediment-laden sea ice with similar reflectivity, and (3) sea ice with relatively low sediment content and clean sea ice, are used to test the classification ability of the reflectance of three bands and the three defined classification indices (Fig. 4). Sample areas were selected from the Chukchi Sea, northern Canada, and Laptev Sea.

As shown in Fig. 4, in Case 1, except for the classification index R_{14}, the reflectance of sediment-laden sea ice and clean sea ice can be completely distinguished using other five indices. In Case 2, it can be seen that R_1, R_3, and R_4 are unable to classify clean sea ice and sediment-laden sea ice because their reflectance is very similar. In Case 3, it can be seen that only the classification index R_{34} is able to distinguish clean sea ice from sea ice with a small sediment content.

Thus, we choose R_{34} as the classification index to distinguish clean sea ice from sediment-laden sea ice. The classification index R_{34} was referred as sediment-laden sea ice-index (SLSI-index) hereby, ranging from –1 to 1. According to Fig. 4, we set the classification threshold to 0. That is, the classification index larger than 0 refers to the sediment-laden sea ice, otherwise, it is classified as clean sea ice.

During the Arctic melt season, pixels within the study area may appear to be mixed with open water and ice floes at the MODIS 500 m spatial resolution. However, the classification index, SLSI-index, was primarily defined utilizing features from the third and fourth bands of MODIS. Both open water and clean sea

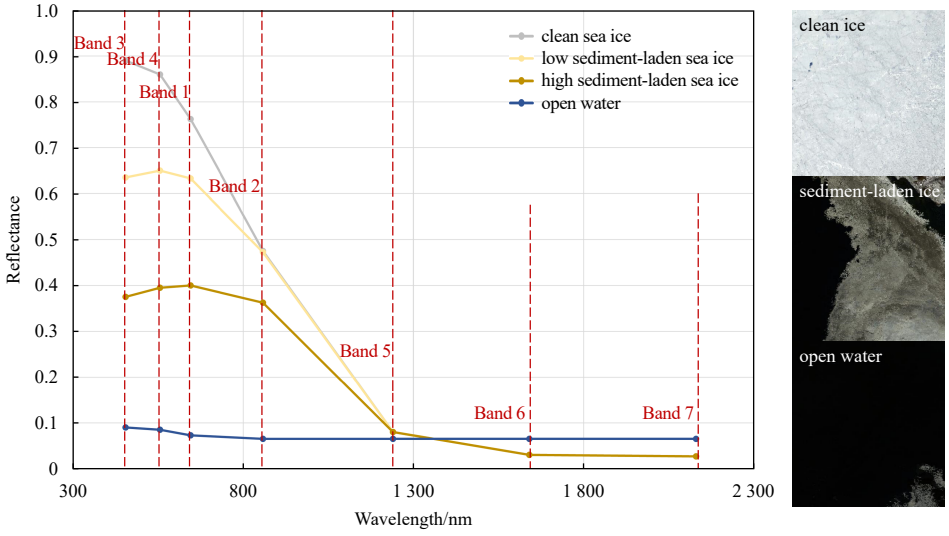

Fig. 3. Reflectance of various surface features (left) and corresponding MODIS true color sub-scenes (right).

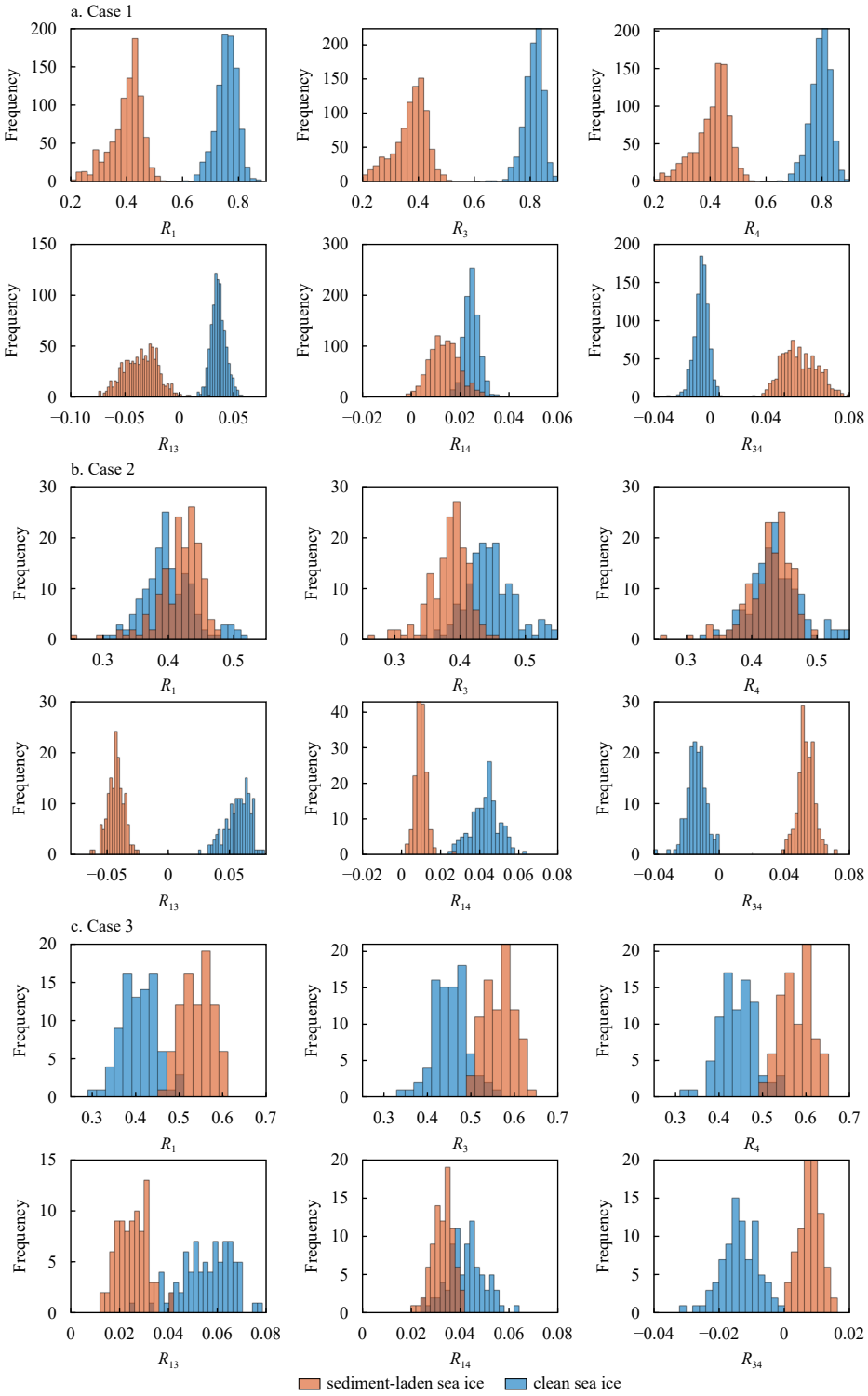

Fig. 4. Histograms of frequency distributions of reflectance of MODIS Bands 1, 3, and 4 and three defined classification indices for three mixed pixel cases.

ice exhibit higher reflectance in MODIS's third band than in its fourth band (Fig. 3), resulting in similar characteristics for their mixed pixels. This feature is opposite to that of sediment-laden sea ice in the third and fourth bands of MODIS. Consequently, this classification method does not misidentify mixed pixels of open water and clean sea ice as sediment-laden sea ice, which has been confirmed by the later validation of the classification results. For the mixed pixels with sediment-laden sea ice and other surface features, the classification result depends on the relative contributions of the features within the pixel, determined by the relative area and spectral contributions.

4 Results and discussion

4.1 *Verification using Landsat-8 images and ship-based photos*

The features of land, clouds and open water are relatively easy

to be distinguished. Here, Landsat-8 true color images with a resolution of 30 m are further used to test the accuracy of the classification results of sediment-laden sea ice from clean sea ice using the MOD09A1 data. Figure 5 presents the MODIS true color image on 18 June 2018 and a scene of Landsat-8 true color images located on the red star in the MODIS image. Figures 5c and d are taken from Landsat-8 and MODIS images at the same location, respectively, and are marked with blue star in Fig. 5b. It can be seen that Landsat-8 images provide more detailed information of the sea ice surface for a better classification of sea ice surface types.

We validated the classification results using 1 042 Landsat-8 ground truth points collected during 2017 to 2021, focusing on the high-incidence regions of sediment-laden sea ice as shown in Fig. 2, the confusion matrix, overall accuracy, and Kappa coefficient are used to quantify the accuracy of our classification method of sediment-laden ice from clean sea ice (Table 1).

The overall accuracy is 92.3% and the Kappa coefficient is 0.84, both of which indicate good performance of our classification method. Furthermore, a widely used and well performed unsupervised classification method, k-means, is conducted on the original MOD09A1 data for comparison. The overall accuracy and Kappa coefficient obtained from k-means is 77.4% and 0.55, respectively. Its relatively low accuracy, compared to our method, is probably due to a lot of misclassifications of clean sea ice as sediment-laden sea ice. Reasons for misclassification might include: (1) different types of sea ice could not be well distinguished by using MOD09A1 data alone, (2) more indices (e.g., bands ratio) should be introduced to improve its accuracy, and (3) the unsupervised classification method was limited by center of clustering, which is unrepresentative in case that the difference between features are not obviously.

In total, 27 photographs taken on board during CHINARE-2018 can match the MODIS observations and were used to verify the sediment-laden sea ice classification. These photographs were obtained in the region near 74°N, 172°W on August 3, 2018. Moreover, clean sea ice in the region near 75°N, 172°W were also observed on the same date. Since the locations where these photographs collected are very centralized and marked in Fig. 6 with red and blue stars, respectively.

As shown in Fig. 6c, the location marked by the red star near the north edge of the region with the sediment-laden sea ice in the classification image, which matches the observation on board. The location marked by the blue star which was classified as clean sea ice also matched the observations on board. Thus, although the number of matched images obtained from ship-based observations is very limited, the northern boundary of sediment-laden sea ice identified by our method based on MOD09A1 data can be considered reasonable.

4.2 *Spatial distribution and temporal variations of sediment-laden sea ice*

The classification results from early May to early September during 2000 to 2021 were obtained. Taking the classification results in 2018 as an example (Fig. 7), sediment-laden sea ice mainly occurs in the marginal seas of the Arctic Ocean, i.e., the Chukchi Sea and coastal seas of Siberia.

The seasonal variations of area fractions in sediment-laden sea ice, clean ice, open water and cloud during 2000–2021, which defined as the percentage relative to the entire study area (Fig. 1), were presented in Fig. 8. As the Arctic sea ice retreats since early May, the fraction of open water continued to increase. However,

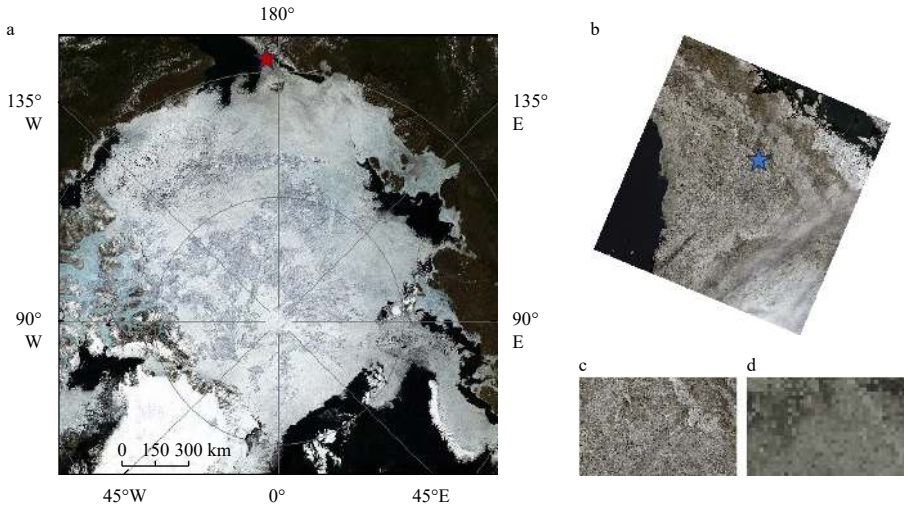

Fig. 5. MOD09A1 and Landsat-8 true color images on 18 June 2018. a and b. Original scenes of MOD09A1 and Landsat-8; c and d. cropped sub-scenes from Landsat-8 and MOD09A1, respectively; the red star marks the location of b. The blue star marks the location of c and d.

Table 1. Confusion matrix for the classification results using proposed method compared with those based on Landsat-8 images during 2017 to 2021

Classification result	Ground truth			
	Clean sea ice	Sediment-laden sea ice	Sum	User accuracy/%
Clean sea ice	559	41	600	93.2
Sediment-laden sea ice	39	403	442	91.2
Sum	598	444	1 042	
Producer accuracy/%	93.5	90.8		

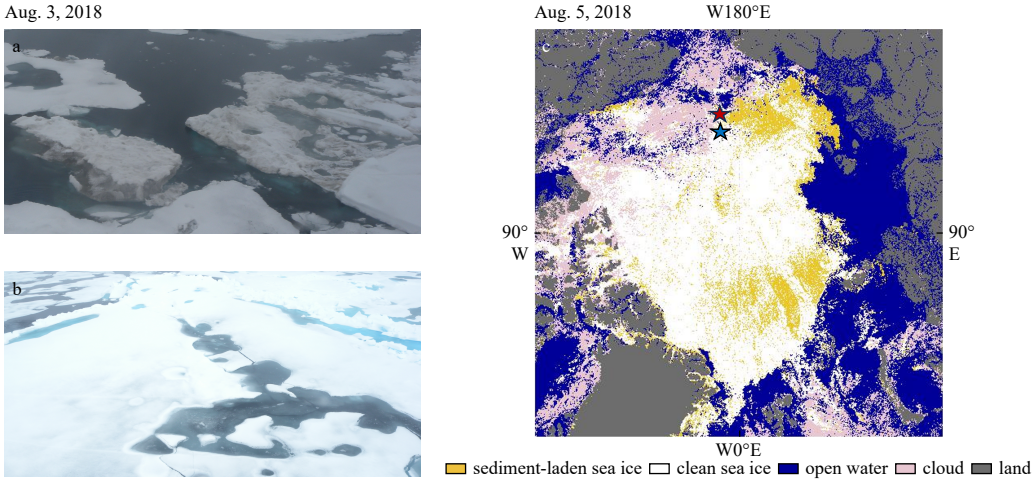

Fig. 6. Sediment-laden sea ice photograph (a) and clean sea ice photograph (b) taken on board R/V *Xuelong* on August 3, 2018 and the corresponding classified result of MODIS obtained on August 5, 2018 (c). The red and blue stars mark the locations where the photographs were taken for sediment-laden sea ice and clean sea ice, respectively.

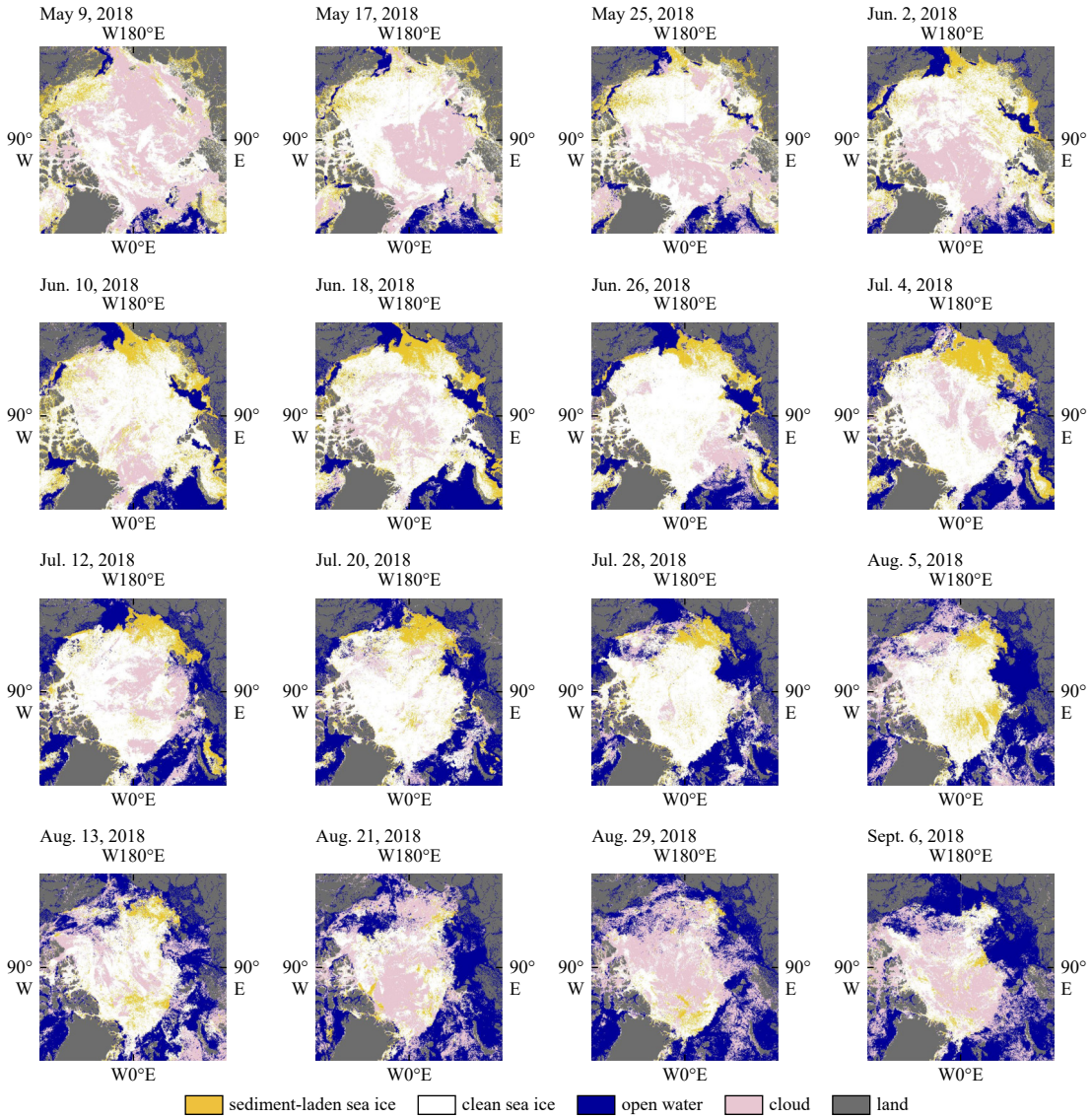

Fig. 7. Classification results of the Arctic Ocean during May to September in 2018.

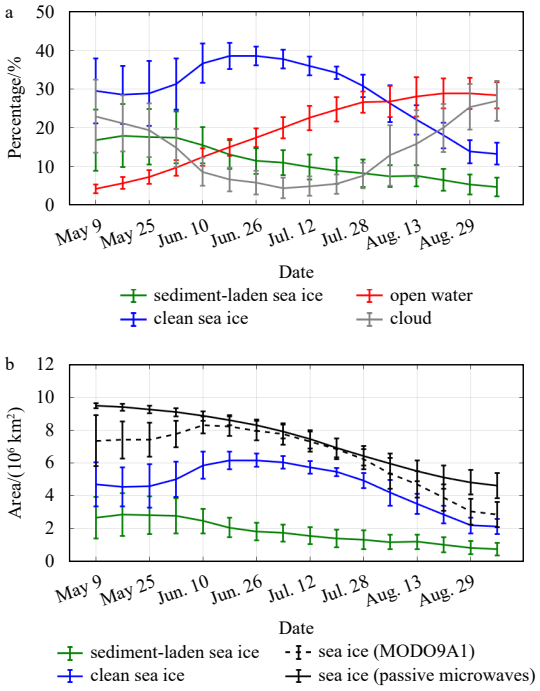

Fig. 8. Seasonal variation of the averages and standard deviations for area fraction (a) and actual area (b) of sediment-laden sea ice, clean sea ice, open water, and cloud, and total sea ice in the study area during 2000–2021.

due to the more frequent cyclone activity in early summer (May) and increase in evaporation during the later summer (August) (Curry et al., 1996), the increasing trend was disturbed by the frequent emergence of clouds. Relatively larger area fractions of cloud were observed in May (21.7%) and August (18.2%), compared to the relatively lower values in June and July (7.2%). The presence of clouds could obscure identifications of the surface features. Thus, a noticeably deviation between the sea ice coverages observed by optical remote sensing (clean ice + dirty ice, with potential impacts of clouds) and by passive microwave remote sensing (total sea ice) is found in May and August, with an average of 21.0%. This deviation decreased significantly in June and July, with an average of 4.9%. It implies that the impact of clouds on identifying sediment-laden ice based on optical remote sensing is trivial in June and July.

The area fraction of clean sea ice shows a trend of increasing prior to mid-June and then decreased, possibly due to high cloud coverage in May and the retreat of sea ice after mid-June. The area fraction of sediment-laden sea ice slightly increased in May, which is likely related to seasonally enhanced snow melting in the Arctic Ocean (e.g., Lei et al., 2022), resulting in early-enriched sediment exposed on the ice surface. From early June onwards, the area fraction of sediment-laden sea ice decreased gradually, in response to the decrease in sea ice area across the pan Arctic Ocean. Note that, the increase in area fraction of cloud may also lead to a decrease in the area fraction of sediment-laden ice to some extent. However, we argue that, this impact is relatively trivial because the high incidence areas of cloud are mainly in the Atlantic sector of the Arctic Ocean (Fig. 7), which is related to the main northward path of extratropical cyclone activity (Liang et al., 2023). While, the high incidence areas of sediment-laden ice, were mainly close to the coasts of the Pacific and the Siberian sectors of the Arctic Ocean. Seasonally, the maximum (2.86×10^6 km^2) area of sediment-laden ice occurred in mid-May. By late August, it decreased to 8.39×10^5 km^2. The sediment-laden ice areas might be underestimated due to the impact of cloud. If we assume that cloud coverage is spatially uniform, then these two values will probably increase by 21.1% and 25.3% (i.e., fraction of cloud coverage), respectively. However, such underestimations are overly exaggerated. Instead, they should be much smaller because of the inconsistency between regions with high cloud coverage (mainly the Arctic Center region) and high sediment-laden ice area fraction (mainly the Arctic marginal seas).

Spatially, although the central Arctic Ocean is not a high-incidence area for sediment-laden ice, we still can clearly identify the traces of dirty ice in the Arctic transpolar-stream region, even extending to Greenland and Barents seas, with the highest probability of occurrence of 21% as shown Fig. 9a. This clearly demonstrates the advection effect of the transpolar stream on ice floes and the sediments originating from the Siberian shelf. The obser-

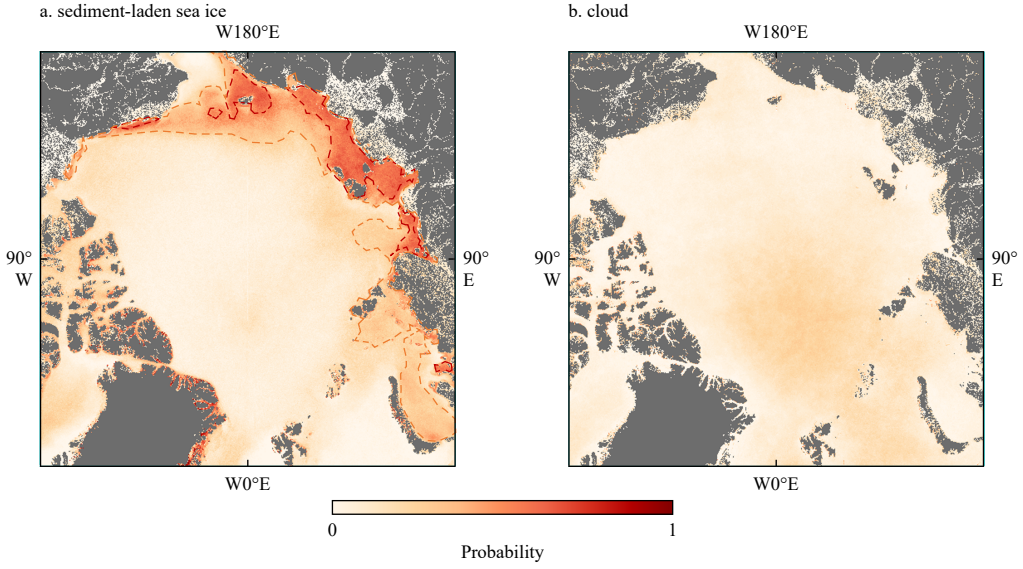

Fig. 9. Probability of occurrence of sediment-laden sea ice and clouds at each grid in June and July during 2000–2021. The orange and red dashed lines in a are the 25% and 50% contour lines, respectively.

vations during the Multidisciplinary drifting Observatory for the Study of Arctic Climate (MOSAiC) expedition conducted in the transpolar-stream region also confirm the existence of sediment-laden ice in this so-called conveyor-belt region of Arctic sea ice (Krumpen et al., 2020). As stated by Krumpen et al. (2019), as Arctic sea ice thins and its residual time over the Arctic basin decreases, sediment carried by ice floes from the Siberian coast may not be able to be transported out of the Arctic Ocean, but melt in the central basin instead, thereby strengthening material exchange between the shelf and the basin.

Since the area fraction of sediment-laden sea ice obtained in June and July is more reliable relative to those in May and August, due to the reduction of cloudy weather in mid-summer, data obtained in June and July during 2000 to 2021 were used to calculate the probability of the occurrence of sediment-laden sea ice at each grid for further analysis (Fig. 9a).

As shown in Fig. 9b, the cloud coverage was less and its distribution was more evenly in June and July, with a relatively high occurrence probability ranging from 2% to 8% in the regions close to the coast of the Pacific and Siberian sectors of Arctic Ocean and had less influence on the identification of spatial pattern of the occurrence probability of sediment-laden sea ice. Spatially, it can be seen that the sediment-laden sea ice was mainly distributed in the Arctic peripheral seas close to the shore, especially in the Chukchi, Eastern Siberian, Laptev, and Kara seas. Sediment-laden sea ice in these regions counts for 57.5% of the total sediment-laden ice over the pan Arctic Ocean (Table 2). While, in the Beaufort Sea, sediment-laden sea ice only occurred in narrow regions close to the coast, and its proportion relative to the total sediment-laden ice area is relatively low (7.8%). Firstly, sediment from rivers facilitates the formation of sediment-laden sea ice. Compared to the Mackenzie River in the Beaufort Sea area, the Yenisei River, Ob River, and Lena River along the Siberian coast have larger discharge volumes (Feng et al., 2021; Yi et al., 2023) and higher sediment loads (Syvitski, 2002; Gordeev, 2006), thereby promoting the formation of sediment-laden sea ice more effectively. In addition, seafloor-carried sediments are the primary sources of particles entrained in sea ice (Ito et al., 2019). The IBCAO Arctic Ocean seafloor topographic were used to analyze the relationship between the spatial distribution of sediment-laden sea ice and the bathymetry (not shown). The shallow seawater and wide continental shelf in Chukchi Sea and the coastal seas of Siberia are beneficial for more sediment being entrapped in the ice during its initial growth. In contrast, sediment-laden sea ice is less distributed in the Beaufort Sea because of the relative narrow continental shelf.

In addition, the interannual variations of different features were analyzed by averaging data in June and July in each year (Fig. 10). During 2000 to 2021, there is a significantly increasing trend with 0.30% per year for the open water area fraction ($P < 0.05$), which is consistent with the decreasing trend of 0.37% per year for the total Arctic sea ice area fraction ($P < 0.05$). Sediment-laden sea ice area reveals a more significantly decreasing trend of 0.56% per year ($P < 0.05$). This type of sea ice mainly appears in the marginal seas of the Arctic Ocean, where the most significant loss of summer sea ice occurs. During 2000–2021, the area fraction of sediment-laden ice decreased from 19.1% (or 3.06×10^6 km^2) to 7.6% (or 1.21×10^6 km^2), with the minimum area of sediment-laden sea ice occurring in 2020 (5.6% or 8.96×10^5 km^2). This decreasing trend further confirms that sediments, attached to the ice floes, might be increasingly difficult to be exported out of the Arctic Ocean through ice advection, but tend to deposit into the Arctic Ocean with the melting of sea ice instead.

In June and July, sediment-laden sea ice area shows a similar trend with the sea ice extent (Fig. 11). The June–July area of Arctic sediment-laden ice mainly depends on the total Arctic extent in the same period. At this time (June–July), the correlation coefficient between these two variables is 0.60 ($P < 0.05$). However, the June–July sediment-laden sea ice area and the averaged sea ice extent from June to annual minimum (September) changed to be weakly correlated, with a correlation coefficient of 0.42 ($P < 0.05$). Furthermore, the correlation coefficient between the detrended time series of June–July sediment-laden ice area and annual minimum sea ice extent (occurring in September) was reduced to 0.33, which was insignificant at the 0.05 confidence

Table 2. Proportion of the regional sediment-laden sea ice area in various Arctic peripheral seas relative to regional sea ice area and total sediment-laden ice area over the Arctic Ocean in June and July during 2000–2021

Arctic peripheral seas	Proportion relative to regional sea ice area/%	Proportion relative to total sediment-laden sea ice area/%
Beaufort Sea	16.4	7.8
Chukchi Sea	29.4	11.1
Eastern Siberian Sea	35.9	18.0
Laptev Sea	45.1	14.9
Kara Sea	51.1	13.5

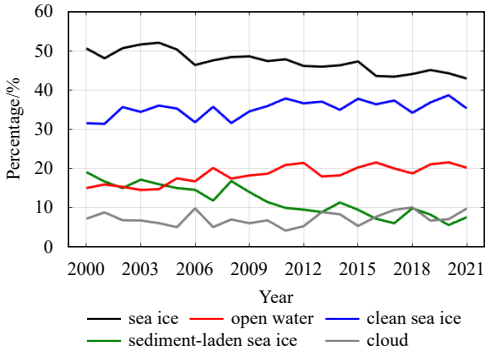

Fig. 10. Interannual variations for area fractions of sea ice, sediment-laden sea, clean sea ice, open water and cloud averaged in June and July during 2000–2021.

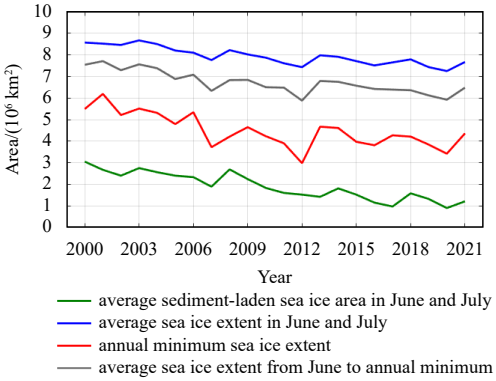

Fig. 11. Interannual variations for average sediment-laden sea ice area in June and July, average sea ice extent in June and July, annual minimum sea ice extent and average sea ice extent from June to the time with annual minimum ice extent during 2000–2021.

level. In the early summer (June–July), dirty ice itself can enhance the ice-albedo positive feedback and promote further ice melt and loss. From this perspective, the June–July area of sediment-laden ice should have a negative impact on the September Arctic sea ice extent. However, such ice-albedo positive feedback caused by dirty ice cannot completely overturn the preconditioned effect of the June–July Arctic sea ice extent on its annual minimum in September. Therefore, the sediment-laden ice area in early summer cannot be used for predicting the Arctic annual minimum ice extent as the melt pond coverage (e.g., Liu et al., 2015), which is likely because sediment-laden ice is often limited to coastal areas and not widely distributed over the pan Arctic Ocean. Therefore, it cannot stimulate a strong albedo positive feedback mechanism as the melt ponds do.

4.3 *Implication of sediment-laden ice on surface albedo*

Sediment-laden sea ice contains sediment and other components that darken its surface and reduce surface albedo. These sediment components enhance the absorption of solar radiation, which accelerates the melting of sea ice (Ledley and Pfirman, 1997). In order to explore the effect of sediment composition on sea ice albedo, we first estimate the albedo approximately using the reflectance of three visible bands of MODIS:

$$\alpha_{\mathrm{vis}} = 0.331\alpha_1 + 0.424\alpha_3 + 0.246\alpha_4, \tag{4}$$

where, α_{vis} represents the estimated regional albedo, and α_1, α_3, and α_4 represents the reflectance of Bands 1, 3 and 4, respectively. Using this formula to simulate the full-band albedo, the R^2 and residual standard error (RSE) can reach 0.999 9 and 0.001 7 respectively, because the spectral pattern of albedo can be greatly sharpened by the reflectance of these bands (Liang, 2001). In order to minimize the effect of clouds, we also choose the June–July data for analysis here.

Using the area fractions of sediment-laden sea ice (A_{si}), clear sea ice (A_{ci}), and open water (A_{ow}), we also estimated the albedo of the study region by neglecting the areas with cloud:

$$\alpha_{\mathrm{reg1}} = A_{\mathrm{si}} \times \alpha_{\mathrm{si}} + A_{\mathrm{ci}} \times \alpha_{\mathrm{ci}} + A_{\mathrm{ow}} \times \alpha_{\mathrm{ow}}, \tag{5}$$

where, α_{reg1} represents the regional albedo without considering the impact of clouds. α_{si}, α_{ci}, and α_{ow} represents the albedo of sediment-laden sea ice, clean sea ice and open water, respectively.

And then, we further estimated the albedo α_{reg2}, neglecting both the contributions from the clouds and the contribution of sediment-laden sea ice.

$$\alpha_{\mathrm{reg2}} = (A_{\mathrm{si}} + A_{\mathrm{ci}}) \times \alpha_{\mathrm{ci}} + A_{\mathrm{ow}} \times \alpha_{\mathrm{ow}}. \tag{6}$$

Through the comparison of estimated regional albedos of α_{vis}, α_{reg1} and α_{reg2} (Fig. 12), we can roughly evaluate the influence of sediment-laden sea ice on surface albedo, and its potential impact on surface shortwave radiation budget.

The June–July averaged α_{vis} is 0.453, which can be considered as the typical value of sea ice with melting snow atop (e.g., Perovich et al., 2002; Lei et al., 2016; Light et al., 2022). Since, there is less cloud coverage (7.2%) in June–July, α_{vis} and α_{reg1} are very close to each other, with an averaged difference of 1.6%. Thus, the impact of clouds on our evaluation of the influence of sediment-laden ice on surface albedo can be ignored. From June to July, the sediment-laden sea ice fraction shows a decreasing trend from 17.4% to 8.2% (Fig. 8a), and its effect on albedo is reflected in the difference between α_{reg1} and α_{reg2} (Fig. 12), which dropped from 22.2% at the beginning of June to 11.9% at the end of July. It implies that the occurrence of sediment-laden sea ice in the Arctic Ocean leads to an average increase of about 14.1% (the ratio of the difference of α_{reg1} and α_{reg2} against the α_{reg1}) in the absorption of solar shortwave radiation by the surface of ice-ocean system. It was noted that this influence was diluted at basin-scale. Locally, the high area fraction of sediment-laden ice in the Siberian coastal region may lead to a maximum decrease in albedo of 22.0%. Low albedo caused by sediment-laden sea ice will inevitably promote the absorption of shortwave radiation, and stimulate local ice-albedo positive feedback though potential acceleration of melting of snow surface and sea ice scattering layer, as well as the formation of melting ponds. Therefore, when using numerical models to estimate the surface heat budget and sea ice mass balance in the Arctic Ocean, the impact of sediment-laden sea ice cannot be ignored, especially in nearshore regions. However, to the best of our knowledge, there is still none of the current climate models considering its impact on surface radiation balance. It might be a way for parameterization optimization in the future.

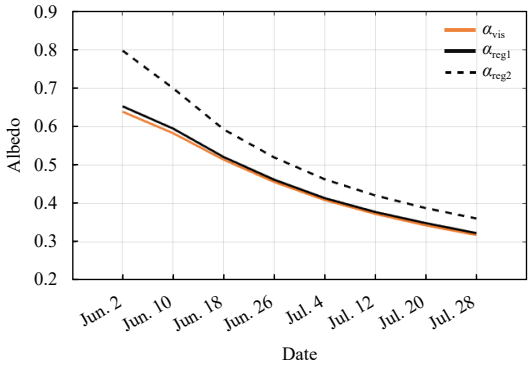

Fig. 12. Seasonal variation of α_{vis}, α_{reg1}, and α_{reg2} within the study region averaged in June and July during 2000–2021.

5 Conclusions

Sediment-laden sea ice is common surface features in the Arctic Ocean, especially in its peripheral seas, and has an important impact on Arctic biogeochemical cycles, as well as the surface shortwave radiation budget. In this study, based on MODIS data, a new classification method for extracting sediment-laden sea ice is proposed by utilizing the difference in spectral characteristics between sediment-laden sea ice and clean sea ice in visible bands. Then, we obtained a time series of sediment-laden sea ice area fraction during 2000–2021. Both Landsat-8 true color images and photographs taken on board verified the accuracy of our method to distinguish sediment-laden sea ice from clean ice. By comparing with the sea ice concentration product of passive microwaves and analyzing cloud coverage and its spatiotemporal variations, the impact of cloud on the identification of sediment-laden sea ice can be weak in June–July.

The results reveal that sediment-laden sea ice is mainly distributed in the Chukchi Sea and Siberian coastal seas, while it is relatively scarce in the Beaufort Sea, probably due to the differences in continental shelf width and river discharge. The area of sediment-laden sea ice in June–July showed a decreasing trend, with a rate of 8.99×10^4 km^2 per year during 2000–2021. The sedi-

ment-laden sea ice would exacerbate the decline in summer sea ice albedo, which enhances the absorption of solar radiation and affects the ice-albedo feedback. From June to July, the occurrence of sediment-laden sea ice over the Arctic Ocean leads to the increased absorption of solar shortwave radiation at the surface of ice-ocean system by about 14.1% on average. However, the coverage of sediment-laden sea ice in early summer still cannot be used as a predictive factor for the annual minimum Arctic sea ice extent because its limited spatial distribution. This study may contribute to further research on sediment transport and biogeochemical cycling in Arctic Ocean, as well as the annual cycle and long-term mass loss of sea ice. In climate models, it is important to consider the impact of sediment-laden sea ice on the parameterization of surface albedo.

6 Outlook

We also acknowledge that it is necessary to combine other satellite data to improve the recognition ability of sediment-laden sea ice in cloud-covered areas, and to obtain more aerial or ship-based observations, and ice and snow samples collected on site to further evaluate and optimize remote sensing retrieval algorithms. The mechanism of sediment-laden ice formation, its relationship with suspended sediment concentration, hydrological processes and runoff features in sea ice formation regions, as well as the relationship between horizontal advection and redistribution of sediment-laden ice and large-scale atmospheric and oceanic circulations, are also important scientific issues that need to be addressed.

References

Arrigo K R. 2014. Sea ice ecosystems. Annual Review of Marine Science, 6: 439–467, doi: 10.1146/annurev-marine-010213-135103

Barber D G, Harasyn M L, Babb D G, et al. 2021. Sediment-laden sea ice in southern Hudson Bay: Entrainment, transport, and biogeochemical implications. Elementa: Science of the Anthropocene, 9(1): 00108, doi: 10.1525/elementa.2020.00108

Bliss A C, Anderson M R. 2018. Arctic sea ice melt onset timing from passive microwave-based and surface air temperature-based methods. Journal of Geophysical Research: Atmospheres, 123(17): 9063–9080, doi: 10.1029/2018JD028676

Brest C L, Rossow W B. 1992. Radiometric calibration and monitoring of NOAA AVHRR data for ISCCP. International Journal of Remote Sensing, 13(2): 235–273, doi: 10.1080/01431169208904037

Cornish S B, Johnson H L, Mallett R D C, et al. 2022. Rise and fall of sea ice production in the Arctic Ocean's ice factories. Nature Communications, 2022(13): 7800, doi: 10.1038/s41467-022-34785-6

Curry J A, Schramm J L, Rossow W B, et al. 1996. Overview of Arctic cloud and radiation characteristics. Journal of Climate, 9(8): 1731–1764, doi: 10.1175/1520-0442(1996)009<1731:OOACAR>2.0.CO;2

Darby D A, Myers W B, Jakobsson M, et al. 2011. Modern dirty sea ice characteristics and sources: The role of anchor ice. Journal of Geophysical Research: Oceans, 116(C9): C09008

Drusch M, Del Bello U, Carlier S, et al. 2012. Sentinel-2: ESA's optical high-resolution mission for GMES operational services. Remote Sensing of Environment, 120: 25–36, doi: 10.1016/j.rse.2011.11.026

Eicken H, Gradinger R, Gaylord A, et al. 2005. Sediment transport by sea ice in the Chukchi and Beaufort Seas: Increasing importance due to changing ice conditions?. Deep-Sea Research Part II: Topical Studies in Oceanography, 52(24–26): 3281–3302, doi: 10.1016/j.dsr2.2005.10.006

Eicken H, Kolatschek J, Freitag J, et al. 2000. A key source area and constraints on entrainment for basin-scale sediment transport by Arctic sea ice. Geophysical Research Letters, 27(13): 1919–1922, doi: 10.1029/1999GL011132

Feng Dongmei, Gleason C J, Lin Peirong, et al. 2021. Recent changes to Arctic river discharge. Nature Communications, 12(1): 6917, doi: 10.1038/s41467-021-27228-1

Fang Shenghui, Zhang Jiajin. 2007. Spectral property analysis of water suspended sediment concentrations. Journal of Geomatics (in Chinese), 32(6): 47–49

Gordeev V V. 2006. Fluvial sediment flux to the Arctic Ocean. Geomorphology, 80(1/2): 94–104, doi: 10.1016/j.geomorph.2005.09.008

Grenfell T C. 1991. A radiative transfer model for sea ice with vertical structure variations. Journal of Geophysical Research: Oceans, 96(C9): 16991–17001, doi: 10.1029/91JC01595

Holmes R M, McClelland J W, Peterson B J, et al. 2002. A circumpolar perspective on fluvial sediment flux to the Arctic Ocean. Global Biogeochemical Cycles, 16(4): 45–1-45-14

Huck P, Light B, Eicken H, et al. 2007. Mapping sediment-laden sea ice in the Arctic using AVHRR remote-sensing data: Atmospheric correction and determination of reflectances as a function of ice type and sediment load. Remote Sensing of Environment, 107(3): 484–495, doi: 10.1016/j.rse.2006.10.002

Irons J R, Dwyer J L, Barsi J A. 2012. The next Landsat satellite: the Landsat data continuity mission. Remote Sensing of Environment, 122: 11–21, doi: 10.1016/j.rse.2011.08.026

Ito M, Ohshima K I, Fukamachi Y, et al. 2019. Favorable conditions for suspension freezing in an arctic coastal Polynya. Journal of Geophysical Research: Oceans, 124(12): 8701–8719, doi: 10.1029/2019JC015536

Jakobsson M, Mayer L A, Bringensparr C, et al. 2020. The international bathymetric chart of the Arctic Ocean version 4.0. Scientific Data, 7(1): 176, doi: 10.1038/s41597-020-0520-9

Ji Lei, Zhang Li, Wylie B. 2009. Analysis of dynamic thresholds for the normalized difference water index. Photogrammetric Engineering & Remote Sensing, 75(11): 1307–1317

Kanna N, Toyota T, Nishioka J. 2014. Iron and macro-nutrient concentrations in sea ice and their impact on the nutritional status of surface waters in the southern Okhotsk Sea. Progress in Oceanography, 126: 44–57, doi: 10.1016/j.pocean.2014.04.012

Krumpen T, Belter H J, Boetius A, et al. 2019. Arctic warming interrupts the Transpolar Drift and affects long-range transport of sea ice and ice-rafted matter. Scientific Reports, 9(1): 5459, doi: 10.1038/s41598-019-41456-y

Krumpen T, Birrien F, Kauker F, et al. 2020. The MOSAiC ice floe: sediment-laden survivor from the Siberian shelf. The Cryosphere, 14(7): 2173–2187, doi: 10.5194/tc-14-2173-2020

Laidre K L, Stirling I, Lowry L F, et al. 2008. Quantifying the sensitivity of arctic marine mammals to climate-induced habitat change. Ecological Applications, 18(sp2): S97–S125, doi: 10.1890/06-0546.1

Ledley T S, Pfirman S. 1997. The impact of sediment-laden snow and sea ice in the Arctic on climate. Climatic Change, 37(4): 641–664, doi: 10.1023/A:1005354912379

Lei Ruibo, Cheng Bin, Hoppmann M, et al. 2022. Seasonality and timing of sea ice mass balance and heat fluxes in the Arctic transpolar drift during 2019–2020. Elementa: Science of the Anthropocene, 10(1): 000089, doi: 10.1525/elementa.2021.000089

Lei Ruibo, Tian-Kunze X, Leppäranta M, et al. 2016. Changes in summer sea ice, albedo, and portioning of surface solar radiation in the Pacific sector of Arctic Ocean during 1982–2009. Journal of Geophysical Research: Oceans, 121(8): 5470–5486, doi: 10.1002/2016JC011831

Lei Ruibo, Tian-Kunze X, Li Bingrui, et al. 2017. Characterization of summer Arctic sea ice morphology in the 135°–175°W sector using multi-scale methods. Cold Regions Science and Technology, 133: 108–120, doi: 10.1016/j.coldregions.2016.10.009

Liang Shunlin. 2001. Narrowband to broadband conversions of land surface albedo I: Algorithms. Remote Sensing of Environment, 76(2): 213–238, doi: 10.1016/S0034-4257(00)00205-4

Liang Yu, Bi Haibo, Lei Ruibo, et al. 2023. Atmospheric latent energy transport pathways into the arctic and their connections to sea ice loss during winter over the observational period. Journal of

Climate, 36(19): 6695–6712, doi: 10.1175/JCLI-D-22-0789.1
Light B, Eicken H, Maykut G A, et al. 1998. The effect of included participates on the spectral albedo of sea ice. Journal of Geophysical Research: Oceans, 103(C12): 27739–27752, doi: 10.1029/98JC02587
Light B, Smith M M, Perovich D K, et al. 2022. Arctic sea ice albedo: Spectral composition, spatial heterogeneity, and temporal evolution observed during the MOSAiC drift. Elementa: Science of the Anthropocene, 10(1): 000103, doi: 10.1525/elementa.2021.000103
Liu Jiping, Song Mirong, Horton R M, et al. 2015. Revisiting the potential of melt pond fraction as a predictor for the seasonal Arctic sea ice extent minimum. Environmental Research Letters, 10(5): 054017, doi: 10.1088/1748-9326/10/5/054017
Markus T, Cavalieri D J, Tschudi M A, et al. 2003. Comparison of aerial video and Landsat 7 data over ponded sea ice. Remote Sensing of Environment, 86(4): 458–469, doi: 10.1016/S0034-4257(03)00124-X
McFeeters S K. 1996. The use of the normalized difference water index (NDWI) in the delineation of open water features. International Journal of Remote Sensing, 17(7): 1425–1432, doi: 10.1080/01431169608948714
Nomura D, Nishioka J, Granskog M A, et al. 2010. Nutrient distributions associated with snow and sediment-laden layers in sea ice of the southern Sea of Okhotsk. Marine Chemistry, 119(1–4): 1–8, doi: 10.1016/j.marchem.2009.11.005
Perovich D K, Grenfell T C, Light B, et al. 2002. Seasonal evolution of the albedo of multiyear Arctic sea ice. Journal of Geophysical Research: Oceans, 107(C10): SHE 20-1-SHE 20-13
Pfirman S L, Eicken H, Bauch D, et al. 1995. The potential transport of pollutants by Arctic sea ice. Science of the Total Environment, 159(2–3): 129–146, doi: 10.1016/0048-9697(95)04174-Y
Rösel A, Kaleschke L, Birnbaum G. 2012. Melt ponds on Arctic sea ice determined from MODIS satellite data using an artificial neural network. The Cryosphere, 6(2): 431–446, doi: 10.5194/tc-6-431-2012
Simpkins G. 2020. Sediment-laden sea ice. Nature Reviews Earth & Environment, 1(1): 9
Stierle A P, Eicken H. 2002. Sediment inclusions in Alaskan coastal sea ice: Spatial distribution, interannual variability, and entrainment requirements. Arctic, Antarctic, and Alpine Research, 34(4): 465–476
Sumata H, de Steur L, Divine D V, et al. 2023. Regime shift in Arctic Ocean sea ice thickness. Nature, 615(7952): 443–449, doi: 10.1038/s41586-022-05686-x
Syvitski J P M. 2002. Sediment discharge variability in Arctic rivers: implications for a warmer future. Polar Research, 21(2): 323–330, doi: 10.3402/polar.v21i2.6494
Tucker W B, Gow A J, Meese D A, et al. 1999. Physical characteristics of summer sea ice across the Arctic Ocean. Journal of Geophysical Research: Oceans, 104(C1): 1489–1504, doi: 10.1029/98JC02607
Vermote E. 2021. MODIS/terra surface reflectance 8-day L3 global 500m SIN grid V061. NASA EOSDIS Land Processes Distributed Active Archive Center
Waga H, Eicken H, Light B, et al. 2022. A neural network-based method for satellite-based mapping of sediment-laden sea ice in the Arctic. Remote Sensing of Environment, 270: 112861, doi: 10.1016/j.rse.2021.112861
Webster M A, Rigor I G, Perovich D K, et al. 2015. Seasonal evolution of melt ponds on Arctic sea ice. Journal of Geophysical Research: Oceans, 120(9): 5968–5982, doi: 10.1002/2015JC011030
Wegner C, Wittbrodt K, Hölemann J A, et al. 2017. Sediment entrainment into sea ice and transport in the transpolar drift: A case study from the Laptev Sea in winter 2011/2012. Continental Shelf Research, 141: 1–10, doi: 10.1016/j.csr.2017.04.010
Yi Shuang, Saemian P, Sneeuw N, et al. 2023. Estimating runoff from pan-Arctic drainage basins for 2002–2019 using an improved runoff-storage relationship. Remote Sensing of Environment, 298: 113816, doi: 10.1016/j.rse.2023.113816
Zhang Fanyi, Pang Xiaoping, Lei Ruibo, et al. 2022. Arctic sea ice motion change and response to atmospheric forcing between 1979 and 2019. International Journal of Climatology, 42(3): 1854–1876, doi: 10.1002/joc.7340
Zhang Na, Wu Yongheng, Zhang Qinghe. 2015. Detection of sea ice in sediment laden water using MODIS in the Bohai Sea: a CART decision tree method. International Journal of Remote Sensing, 36(6): 1661–1674, doi: 10.1080/01431161.2015.1015658